Received: 30 January 2020 | Revised: 26 March 2020 | Accepted: 23 April 2020

DOI: 10.1002/adc2.38

ORIGINAL ARTICLE

WILEY

Hybrid nonlinear observer for battery state-of-charge estimation using nonmonotonic force measurements

Hamidreza Movahedi[1] | **Miriam A. Figueroa-Santos**[2] | **Jason B. Siegel**[2] | **Anna G. Stefanopoulou**[2] | **Rajesh Rajamani**[1]

[1]Department of Mechanical Engineering, University of Minnesota Twin Cities

[2]Department of Mechanical Engineering, University of Michigan

Correspondence
Rajesh Rajamani, Department of Mechanical Engineering, University of Minnesota Twin Cities, Minneapolis, MN 55455.
Email: rajamani@umn.edu

Funding information
National Science Foundation, Grant/Award Number: CMMI 1562006

This article focuses on state-of-charge (SOC) estimation in a lithium-ion battery, using measurements of terminal voltage and bulk force. A nonlinear observer designed using Lyapunov analysis relying on lower and upper bounds of the Jacobian of the nonlinear output function is utilized. Rigorous analysis shows that the proposed observer has feasible design solutions only in each piecewise monotonic region of the output functions and has no constant stabilizing observer gain when the entire SOC range is considered. The nonmonotonicity challenge is then addressed by designing a hybrid nonlinear observer that switches between several constant observer gains. The global stability of the switched system is guaranteed by ensuring overlap between regions and an adequate dwell time between switches. The performance of the observer is evaluated first through simulations using a high-fidelity battery model and then through experiments. The performance of the nonlinear observer is compared with that of an extended Kalman Filter. Simulation results show that with no model uncertainty the nonlinear observer provides estimates with an RMS error of 1.1%, while the EKF performs better, providing an RMS error less than 1%. However, when model error is introduced into this nonmonotonic system, the EKF becomes unstable for even very small model errors in the output curves. The nonlinear observer, on the other hand, continues to perform very well, providing accurate estimates and never becoming unstable. The experimental results verify the observations from the simulation and the experimental EKF is found to become unstable due to model errors, while the hybrid nonlinear observer continues to work reliably.

KEYWORDS
force sensor, hybrid observer, lithium-ion batteries, nonlinear observer, SOC estimation

1 | INTRODUCTION

1.1 | Background

Lithium-ion cells dominate the battery market for automotive propulsion and for consumer electronics due to their advantages of high energy density and slow self-discharge.[1,2] The state-of-charge (SOC) of a lithium-ion battery is a basic

indicator of the fraction of charge that remains in the battery cells. SOC needs to be estimated accurately in real time, since it is indicative of the remaining range of operation of the battery, which is especially critical in the case of an electrical vehicle. The estimation of SOC, power capability, and cell capacity are important functions of the battery management system, needed to safely manage the cells to prevent overcharging and overdischarging.[3]

SOC is typically estimated using a measurement of the terminal voltage, an electrical circuit model and by effectively inverting the voltage-SOC curves of the battery. In this regard, the sensitivity of the voltage curves to the SOC is very important in order to estimate SOC accurately.[4] In the case of the lithium-ion-iron-phosphate (LFP) battery used in this article, the relationship between voltage and SOC has an almost-flat slope for most of the SOC range (30%-70%), as seen in Figure 3. Hence the estimation of SOC from the voltage measurement is quite difficult under noisy measurements.[4-7] This article, therefore, considers the use of an additional sensor, namely a load cell force sensor, to estimate SOC.

1.2 | Review of state of charge estimation methods

The state of charge (SOC) of a battery is an indicator of the remaining energy in it, and can be defined as:

$$\mathrm{SOC}(t) = 1 - \frac{\int_0^t I \, \mathrm{d}t}{C_n}. \tag{1}$$

Here I is the current supplied by the battery and C_n is the nominal capacity of the battery. While C_n has the SI units of $A.\ secs$ in the above equation, the units of $A.\ hours$ is more typically used to describe a battery's capacity. In general,

$$0 \leq \mathrm{SOC}(t) \leq 1. \tag{2}$$

Different methods for estimating the SOC have been explored in the literature. These include coulomb counting, open circuit voltage measurement, internal resistance measurement, bulk force measurement, and electrochemical impedance spectroscopy. A few of these SOC estimation methods are briefly discussed below.

1.2.1 | Coulomb counting

The easiest method for estimation of SOC is coulomb counting, which is essentially measuring and integrating the current from the battery over time, as in Equation (1). Even though this method seems straightforward, an integrator is a marginally stable dynamic system and is highly prone to drift errors. For example, even a very small bias in current measurement will cause large cumulative errors in the estimator. To prevent drift or to manage drift for long time intervals, the current has to be measured very accurately and further the integral has to be reset each time the battery is fully charged (the only condition in which the SOC is accurately known).

1.2.2 | Open circuit voltage

It has been observed that the open circuit voltage V_{OC} of the battery is an algebraic function of SOC; therefore, the inverse of this function can be utilized in the estimation algorithm. There are three major problems associated with using V_{OC} for SOC estimation[7]:

1. The V_{OC} is quite a sensitive function of SOC at low and high SOC values. But, there are intermediate regions of SOC where V_{OC} is *not* a sensitive function of SOC, as seen in Figure 3A.
2. Sometimes, a significant hysteresis in battery terminal voltage can be observed with respect to SOC.[7]
3. V_{OC} itself cannot be directly measured, but must instead be estimated from the terminal voltage V_{t} of the battery. The relationship between V_{t} and OCV is described in the plant model equations in Section 2.1.

1.2.3 | Bulk force

It has been known that the insertion of lithium ions into the electrode host materials (intercalation and deintercalation) during charging and discharging can cause expansion of the crystal lattice of the material. This expansion of the particles in the electrode results in a volume change of the battery. It was shown by Mohan et al[8] that the force exerted on the casing of the battery as a result of this change in volume is an algebraic function of SOC. Hence, if the bulk force can be measured, the SOC could potentially be estimated from it in real time. The use of bulk force measurements by some of the authors of this article and by others has been previously reported in References [4,8-13]. Model development and validation can be seen in References [12-14]. In the case of the lithium-iron-phosphate (LFP) cathode battery chemistry used in this article and in Reference [4], the relationship between the bulk force and the SOC of the battery is quite nonlinear and nonmonotonic, making the design of the estimation algorithm quite challenging. Previously, this has been handled by using piecewise linearization of the output nonlinear function and use of a traditional Kalman filter.[4]

1.2.4 | Nonlinear observer design

Nonlinear observers and Linear Matrix Inequality (LMI)-based methods of nonlinear observer design have been developed by several researchers in literature, including Arcak and Kokotovic,[15] Phanomchoeng et al,[16] Boizot et al,[17] and Wang et al.[18] However, as will be shown later in Section 3.3, all of these observer design methods from literature fail to yield a feasible constant gain stable observer, when the involved nonlinear function is nonmonotonic. Other advanced estimation techniques have also been explored during the last 15 years.[19-21]

1.3 | Article outline

This article focuses on the use of the terminal voltage and a force sensor with the LFP battery for real-time estimation of the battery SOC. The design of a nonlinear observer, which provides globally stable SOC estimation for the nonlinear system is demonstrated. It turns out that the nonmonotonic nature of the nonlinear function prevents the existence of a single-constant observer gain that can provide stability over the entire operating regime of the battery. Hence, a hybrid observer that uses a finite state machine to switch between a few constant gain nonlinear observers is utilized.

The clear advantages of the new nonlinear observer over a traditional estimation algorithm such as the extended Kalman filter are demonstrated in this article. In particular, model errors in the output nonlinear function coupled with the nonmonotonic nature can easily cause the EKF to diverge. While careful choice of the covariance characteristics for the EKF can be used to prevent divergence, these choices come with significant performance trade-offs. The hybrid nonlinear observer developed in this article, on the other hand, provides accurate and robust performance in the presence of model error, and does not need any careful tuning of parameters.

The outline of the article is as follows: Section 2 presents the dynamic plant model and output functions for the lithium-ion battery used in this study. Section 3 presents the nonlinear observer design method proposed to be used for this plant and also provides an analytical proof that a single constant observer gain over the entire SOC range cannot exist for this system. Section 4 presents the design of a hybrid nonlinear observer that utilizes switched observer gains to obtain global stability. Section 5 presents extensive results from simulation using both the nonlinear observer and an extended Kalman filter (EKF). Section 6 discusses the influence of model error, especially at the zero-slope point for this nonmonotonic system. Section 7 discusses the initial condition and initial gain determination. Section 8 presents experimental results which verify the robustness and performance of the nonlinear observer and its superiority over the EKF. Section 9 contains the conclusions.

2 | LITHIUM-ION BATTERY DYNAMIC MODEL

2.1 | Plant model for observer design

Models with different levels of complexity have been proposed in the literature for the electrical dynamics of lithium-ion batteries.[22-24] Here an equivalent circuit V_{OC}-R-RC-RC model will be used to model the electrical dynamics, as shown in Figure 1.[4]

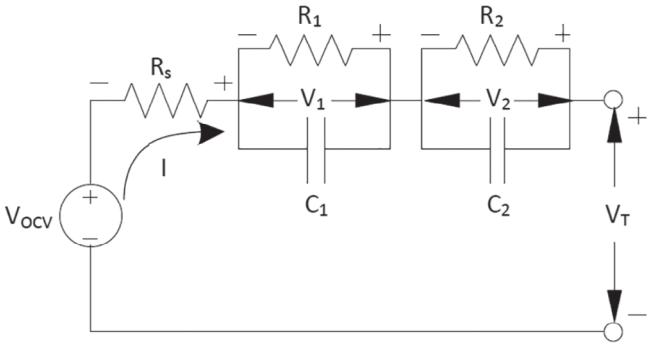

FIGURE 1 V_{OC}-R-RC-RC model for battery[3]

For the model in Figure 1, the dynamic equations of the battery can be represented as[4]:

$$\frac{dV_1}{dt} = \frac{-V_1}{R_1C_1} + \frac{I}{C_1}, \tag{3}$$

$$\frac{dV_2}{dt} = \frac{-V_2}{R_2C_2} + \frac{I}{C_2}, \tag{4}$$

$$\frac{d\,\mathrm{SOC}}{dt} = -\frac{I}{C_n}, \tag{5}$$

where V_1, V_2, and I are voltages and current, as seen in Figure 1, R_1, R_2, C_1, C_2 are electrical model parameters, and C_n is the capacity of the battery. Model development is available in Reference [4] and the references therein.

Two output measurements will be considered here; first the terminal voltage y_1, which is a function of all three states and second, the bulk force y_2, which is assumed to be an algebraic function of the SOC.

$$y_1 = V_t = V_{\mathrm{OC}}(\mathrm{SOC}) - IR - V_1 - V_2, \tag{6}$$

$$y_2 = F = F(\mathrm{SOC}). \tag{7}$$

Thus, considering Equations (3)-(7), the plant model is of the following form:

$$\dot{x} = Ax + Bu, \tag{8}$$

$$y = Cx + h(x), \tag{9}$$

where $x = [V_1\ V_2\ \mathrm{SOC}]^T$, and $y = \begin{bmatrix} y_1 & y_2 \end{bmatrix}^T$. It can be seen that the process dynamics are linear, while the output functions are nonlinear. A six-degree polynomial was used to fit a curve for the nonmonotonic bulk force vs SOC relationship, whose experimental data are shown in Figure 3B:

$$y_2 = F = 755\,\mathrm{SOC}^6 - 2902\,\mathrm{SOC}^5 + 4118\,\mathrm{SOC}^4 - 2564\,\mathrm{SOC}^3 + 590\,\mathrm{SOC}^2 + 26\,\mathrm{SOC} + 1667. \tag{10}$$

Likewise, an algebraic nonlinear monotonic function was fit to the open-circuit voltage data shown in Figure 3A[4]:

$$\begin{aligned} y_1 = V_{\mathrm{OC}} = {} & -2.4354 + 0.1162 \times (1 - \exp(-5.7469 * \mathrm{SOC})) - 0.0098 \times \mathrm{SOC} + 1.2942 \times \left(1 - \exp\left(\frac{3.0014\mathrm{e}-4}{1-\mathrm{SOC}}\right)\right) \\ & + 0.0206 \times \tanh\left(\frac{\mathrm{SOC} - 0.2321}{0.0626}\right) + 5.6185 \times \tanh\left(\frac{\mathrm{SOC} + 0.0513}{0.0406}\right) + 0.0166 \times \tanh\left(\frac{\mathrm{SOC} - 0.6799}{0.0306}\right). \end{aligned} \tag{11}$$

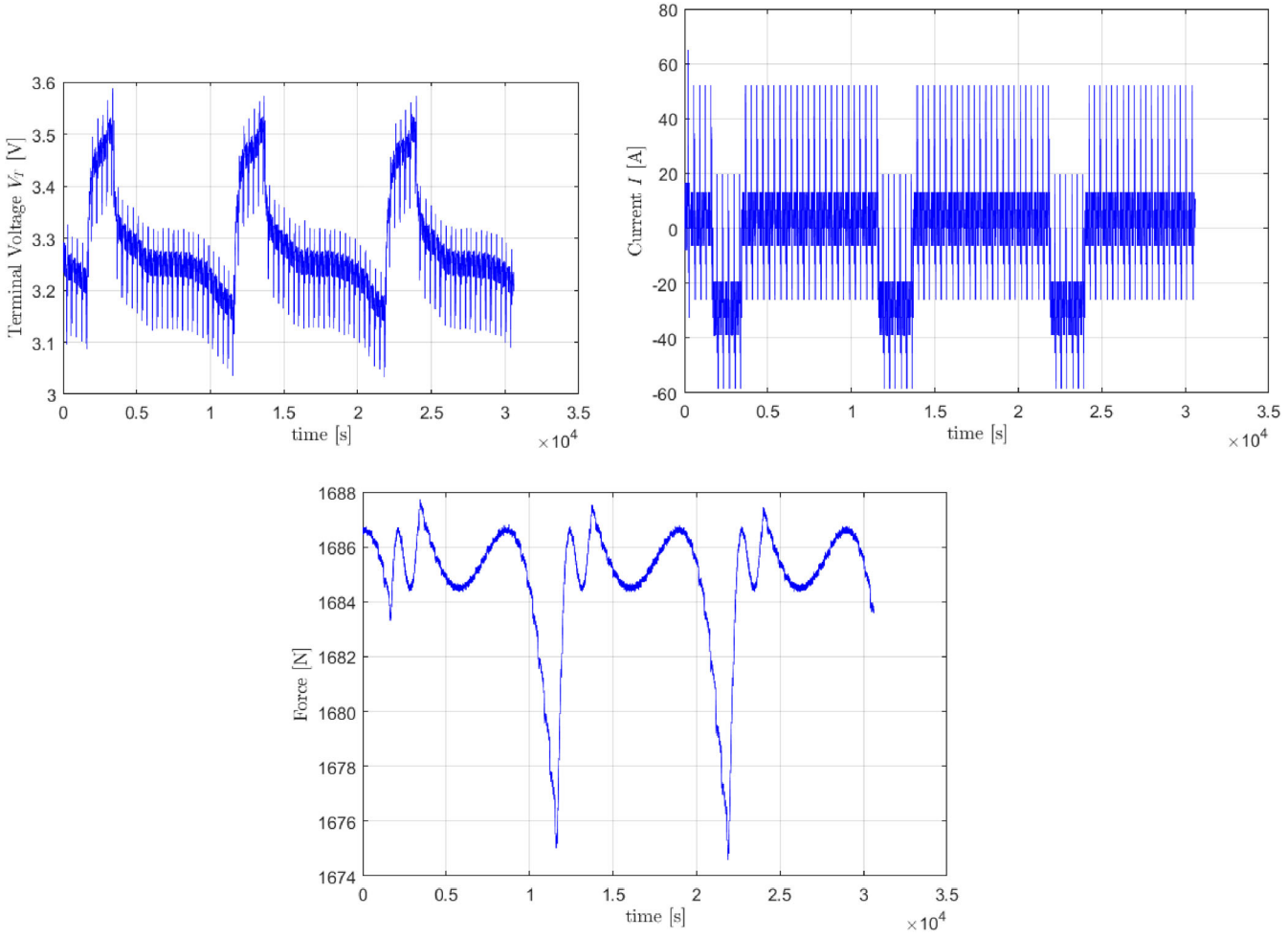

FIGURE 2 Measurements and the input current for simulation studies

2.2 | Simulation model

Although Equations (3)-(7) will constitute the battery model that will be used to design the observer, in order to evaluate the observer in simulations, the following modifications were made to the model for purposes of the simulation:

- A small unknown bias was added to the current (the current was assumed to have a small bias error when its measurement is used in the observer).
- Gaussian noise was added to both measurement signals in the simulations.

The simulated outputs and current input are shown in Figure 2. This simulation scenario consists of multiple cycles of dynamic stress testing (DST), which is a standard procedure to test the performance of a battery on electric vehicles.[24-26] The test consists of a long series of step charge/discharge current inputs with nonzero average that are used back-to-back to charge and discharge a battery. Here we see three rounds of battery charge and discharge in this simulation scenario.

2.3 | Output functions

The two functions $V_{\mathrm{OC}}(\mathrm{SOC})$ and $F(\mathrm{SOC})$ involved in the output equations (6) and (7) are shown as curves in Figure 3.[27] As seen in Figure 3, both these functions are nonlinear functions of SOC. However, $V_{\mathrm{OC}}(\mathrm{SOC})$ can be represented entirely using a monotonic polynomial curve, while the bulk force $F(\mathrm{SOC})$ is clearly a nonmonotonic function.

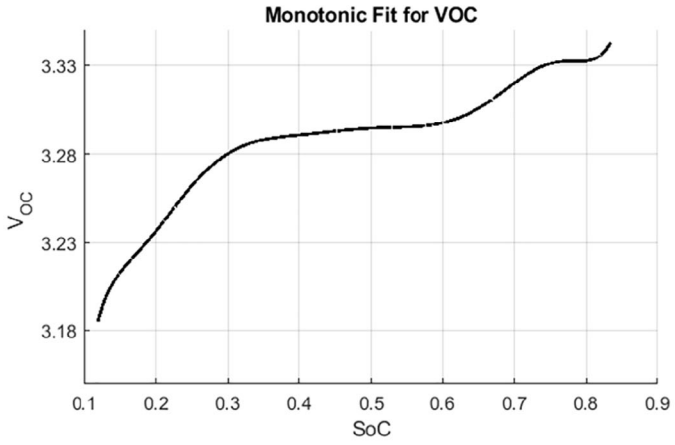

(A) Monotonic fitted curve for Voc

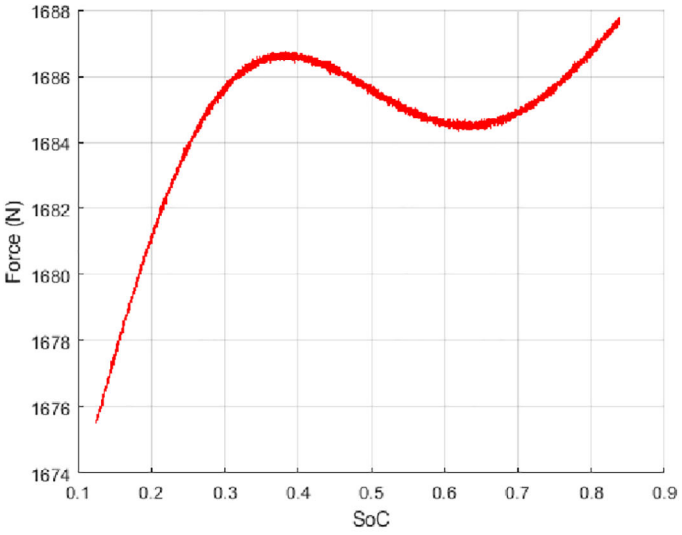

(B) Bulk force measured curve as a function of SoC

FIGURE 3 Output functions for the battery system

3 | NONLINEAR OBSERVER DESIGN

3.1 | Nonlinear observer for bounded Jacobian output functions

For the plant model given by Equations (8)-(9), the following nonlinear observer is proposed:

$$\dot{\hat{x}} = A\hat{x} + Bu + L[y - C\hat{x} - h(\hat{x})]. \tag{12}$$

Let the estimation error be $\tilde{x} = x - \hat{x}$. Then the estimation error dynamics obtained by subtracting Equation (12) from Equation (8) is

$$\dot{\tilde{x}} = (A - LC)\tilde{x} - L[h(x) - h(\hat{x})]. \tag{13}$$

The presence of the nonlinear function $h(x) - h(\hat{x})$ in Equation (13) means a linear observer may not ensure globally stable estimation for this nonlinear system.

It is clear that the system is linear in the process dynamics and has nonlinear measurement equations. Furthermore, the nonlinear functions in the output (measurement) equations are smooth and differentiable with bounded slopes at every operating point. Hence, a nonlinear observer design method that allows a nonlinear function in the output equations and uses the lower and upper bounds on the Jacobian of this nonlinear function is utilized.[18] The key observer design result that will be utilized is as follows:

Theorem 1. *Let K_1 and K_2 be the lower and upper bounds of the Jacobian of the nonlinear function $h(x)$ of Equation* (10) *so that the (i,j)th elements of the matrices K_1 and K_2 satisfy*

$$K_1(i,j) \le \frac{\partial h_i}{\partial x_j} \le K_2(i,j). \tag{14}$$

If the observer gain matrix L and a positive definite matrix P are determined such that they satisfy the following linear matrix inequalities

$$P > 0, \tag{15}$$

$$\begin{bmatrix} (A-LC)^T P + P(A-LC) + \sigma P & -PL \\ -L^T P & 0 \end{bmatrix} - \begin{bmatrix} \frac{K_1^T K_2 + K_2^T K_1}{2} & -\frac{K_1^T + K_2^T}{2} \\ -\frac{K_1 + K_2}{2} & I \end{bmatrix} < 0, \tag{16}$$

then the observer given by Equation (12) is exponentially stable, with an exponential convergence time constant of at least σ.

Proof. This result is based on use of a previous nonlinear observer design method from a theoretical publication of our research group.[18] From theorem 2.1 of Reference [18], if

1. the nonlinearity in the process dynamics is set to zero (ie, $f(x) = 0$),
2. the output error injection in the output nonlinearity is removed (ie, $L_2 = 0$), and
3. the Lyapunov asymptotic stability condition $\dot{V} < 0$ is replaced by the exponential convergence rate condition $\dot{V} < -\sigma V$,

then the observer design condition of Equation (16) can be obtained. ∎

3.2 | Nonexistence of a stable observer due to nonmonotonicity

Theorem 2. *If the nonlinear functions in $h(x)$ are nonmonotonic, then a constant observer gain L that satisfies Equation* (16) *cannot exist*.

Proof. Part 1: In this part, we show that the linear portion of the estimation error dynamics is not stable in this application and can never be stabilized, no matter how the observer gain L is chosen. Hence, the nonlinear output functions are needed for stabilization.

For applying Theorem 1, the system matrices in this application are:

$$A = \begin{bmatrix} -\frac{1}{R_1 C_1} & 0 & 0 \\ 0 & -\frac{1}{R_2 C_2} & 0 \\ 0 & 0 & 0 \end{bmatrix}, \quad B = \begin{bmatrix} \frac{1}{C_1} \\ \frac{1}{C_2} \\ -\frac{1}{C_b} \end{bmatrix},$$

$$h(x) = \begin{bmatrix} V_{\text{oc}}(\text{SOC}) \\ F(\text{SOC}) \end{bmatrix}, \quad C = \begin{bmatrix} -1 & -1 & 0 \\ 0 & 0 & 0 \end{bmatrix}.$$

Let the observer gain be

$$L = \begin{bmatrix} \ell_{11} & \ell_{12} \\ \ell_{21} & \ell_{22} \\ \ell_{31} & \ell_{32} \end{bmatrix}.$$

Then

$$A - LC = \begin{bmatrix} -\frac{1}{R_1 C_1} - \ell_{11} & -\ell_{11} & 0 \\ -\ell_{21} & -\frac{1}{R_2 C_2} - \ell_{21} & 0 \\ -\ell_{31} & -\ell_{31} & 0 \end{bmatrix}.$$

Hence $(A - LC)$ has one eigenvalue at 0 and is not asymptotically stable, no matter how L is chosen. It can also be easily checked that (A, C) is undetectable. Hence, the linear portion of the output cannot stabilize the dynamics and the nonlinear function in the output is needed for stabilization.

Part 2: If the nonlinear output function $F(\text{SOC})$ is nonmonotonic, then

$$K_1 = \begin{bmatrix} 0 & 0 & \frac{\partial V_{oc}}{\partial(\text{SOC})}\Big|_{\min} \\ 0 & 0 & \frac{\partial F}{\partial(\text{SOC})}\Big|_{\min} \end{bmatrix} \tag{17}$$

and

$$K_2 = \begin{bmatrix} 0 & 0 & \frac{\partial V_{oc}}{\partial(\text{SOC})}\Big|_{\max} \\ 0 & 0 & \frac{\partial F}{\partial(\text{SOC})}\Big|_{\max} \end{bmatrix}. \tag{18}$$

Hence

$$K_1^T K_2 = K_2^T K_1 = \begin{bmatrix} 0 & 0 & 0 \\ 0 & 0 & 0 \\ 0 & 0 & \left\{ \frac{\partial V_{oc}}{\partial(\text{SOC})}\Big|_{\min} \right\} \left\{ \frac{\partial V_{oc}}{\partial(\text{SOC})}\Big|_{\max} \right\} + \left\{ \frac{\partial F}{\partial(\text{SOC})}\Big|_{\min} \right\} \left\{ \frac{\partial F}{\partial(\text{SOC})}\Big|_{\max} \right\} \end{bmatrix}.$$

The force measurement nonlinear functions in $h(x)$ $F(\text{SOC})$ is nonmonotonic, so that $\frac{\partial F}{\partial(\text{SOC})}\Big|_{\min} < 0$ and $\frac{\partial F}{\partial(\text{SOC})}\Big|_{\max} > 0$.

Also, the $V_{oc}(\text{SOC})$ curve has almost zero sensitivity in some portions of the SOC range, so that the minimum slope

$$\frac{\partial V_{oc}}{\partial(\text{SOC})}\Big|_{\min} = 0.$$

Furthermore, $\frac{\partial V_{oc}}{\partial(\text{SOC})}\Big|_{\max} > 0$.

Hence, from Equations (17) and (18), $K_1^T K_2 + K_2^T K_1 \leq 0$. This implies

$$\begin{bmatrix} (A - LC)^T P + P(A - LC) + \sigma P & -PL \\ -L^T P & 0 \end{bmatrix} - \begin{bmatrix} \frac{K_1^T K_2 + K_2^T K_1}{2} & -\frac{K_1^T + K_2^T}{2} \\ -\frac{K_1 + K_2}{2} & I \end{bmatrix} < 0$$

if and only if $\begin{bmatrix} (A - LC)^T P + P(A - LC) + \sigma P & -PL \\ -L^T P & 0 \end{bmatrix} < 0$.

In turn, this is possible if and only if

$$(A - LC)^T P + P(A - LC) + \sigma P < 0. \tag{19}$$

But, if $(A - LC)$ is not asymptotically stable for any L (from part 1), then a solution to Equation (19) can never exist.

Hence, this nonlinear observer cannot be stable with a constant observer gain, if the nonlinear function is nonmonotonic. ■

3.3 | Nonexistence of a stable observer from other nonlinear observer results in literature

It can be shown that the following popular methods of observer design for nonlinear systems from literature all fail to yield a solution with a constant observer gain for the nonmonotonic system considered in this article:

1. Observer design method of Arcak and Kokotovic using the Circle Criterion[15]:

The method developed in[15] is also based on the solution to a LMI. But it allows for nonlinear functions only in the process dynamics and not in the output equation. Further, it requires the nonlinear function in the process dynamics to be *monotonic*. Since the system considered in this manuscript has a nonlinear function in the output equation and further the nonlinear function happens to be *nonmonotonic*, the observer design method of[15] is not applicable to this problem.

2. Observer design method of Phanomcheong et al for bounded Jacobian nonlinear systems[16]:

Next, consider the class of systems and observer forms described below, with the plant:

$$\begin{aligned} \dot{x} &= Ax + \Phi(x) + g(y,u) \\ y &= Cx + \Psi(x), \end{aligned} \tag{20}$$

where $x \in R^n$ is the state vector, $u \in R^p$ is the input vector, and $y \in R^m$ is the output measurement vector. $A \in R^{n\times n}$ and $C \in R^{m\times n}$ are appropriate matrices. The functions $\Phi(x) : R^n \to R^n$, $\Psi(x) : R^n \to R^m$, and $g(y,u) : R^m \times R^p \to R^n$ are nonlinear. In addition, $\Phi(x)$ and $\Psi(x)$ are assumed to be differentiable. The observer is assumed to be of the form

$$\begin{aligned} \dot{\hat{x}} &= A\hat{x} + \Phi(\hat{x}) + g(y,u) + L(y - \hat{y}) \\ \hat{y} &= C\hat{x} + \Psi(\hat{x}). \end{aligned} \tag{21}$$

For the class of systems and observer forms described in Equations (18) and (19), according to theorem 2 in Reference [16], if an observer gain matrix L can be chosen such that

$$\begin{gathered} P(A + \overline{H}_{ij}^{\max}) + (A + \overline{H}_{ij}^{\max})^T P - (C + \overline{G}_{kj}^{\max})^T L^T P - PL(C + \overline{G}_{kj}^{\max}) < 0 \\ P(A + \overline{H}_{ij}^{\max}) + (A + \overline{H}_{ij}^{\max})^T P - (C + \overline{G}_{kj}^{\min})^T L^T P - PL(C + \overline{G}_{kj}^{\min}) < 0 \\ P(A + \overline{H}_{ij}^{\min}) + (A + \overline{H}_{ij}^{\min})^T P - (C + \overline{G}_{kj}^{\max})^T L^T P - PL(C + \overline{G}_{kj}^{\max}) < 0 \\ P(A + \overline{H}_{ij}^{\min}) + (A + \overline{H}_{ij}^{\min})^T P - (C + \overline{G}_{kj}^{\min})^T L^T P - PL(C + \overline{G}_{kj}^{\min}) < 0 \\ P > 0 \end{gathered} \tag{22}$$

$\forall i = 1, \ldots, n, \forall j = 1, \ldots, n$, and $\forall k = 1, \ldots, m$, where

(1) $h_{ij}^{\max} \geq \max(\partial\Phi_i/\partial x_j)$ and $h_{ij}^{\min} \leq \min(\partial\Phi_i/\partial x_j)$,
(2) $H_{ij}^{\max} = e_n(i)e_n^T(j)h_{ij}^{\max}$ and $H_{ij}^{\min} = e_n(i)e_n^T(j)h_{ij}^{\min}$,
(3) $z_H = n \times n$ is the state scaling factor, n being dimension of the state vector,
(4) $\overline{H}_{ij}^{\max} = z_H H_{ij}^{\max}$ and $\overline{H}_{ij}^{\min} = z_H H_{ij}^{\min}$,
(5) $g_{kj}^{\max} \geq \max(\partial\Psi_k/\partial x_j)$ and $g_{kj}^{\min} \leq \min(\partial\Psi_k/\partial x_j)$,
(6) $G_{kj}^{\max} = e_n(k)e_n^T(j)g_{kj}^{\max}$and $G_{kj}^{\min} = e_n(k)e_n^T(j)g_{kj}^{\min}$,
(7) $z_G = m \times n$ is the output scaling factor, m being dimension of the output vector,
(8) $\overline{G}_{kj}^{\max} = z_G G_{kj}^{\max}$ and $\overline{G}_{ij}^{\min} = z_G G_{kj}^{\min}$,

then this choice of L leads to asymptotically stable estimates by the observer (21) for the system (20).

It can be seen that if A is not asymptotically stable, and if $\overline{G}_{kj}^{\max} > 0$ and $\overline{G}_{kj}^{\min} < 0$, then there are no feasible solutions to the LMI system (22). When the output nonlinear function is nonmonotonic, then $\overline{G}_{kj}^{\max} > 0$ and $\overline{G}_{kj}^{\min} < 0$. Hence, there are no feasible solutions from the observer design method of Reference [16].

3. High gain observer design method, when the output function is nonmonotonic, as demonstrated in Reference [17]:

The high gain observer design method applies to triangular nonlinear systems, generally after convenient transformation.[17] The high gain observer with a constant gain requires the monotonicity of the output nonlinearity and of some nonlinearities in the process, see Reference [17] and the references therein for systems with single outputs. Without this monotonicity assumption, the exponential convergence of the high-gain observer with a constant gain cannot be proved.

R_1, R_3 R_5: Observer design using both force and voltage feedback

R_2, R_4: Observer design using voltage feedback only

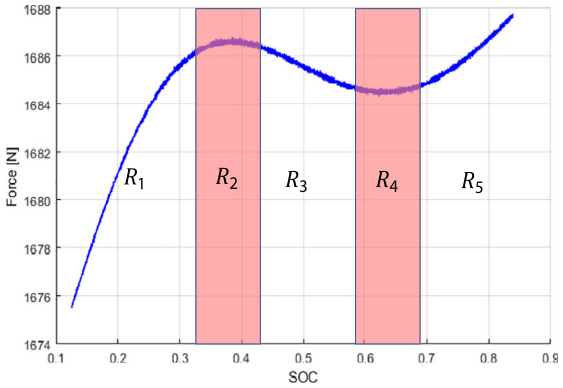

FIGURE 4 Creating regions around slope-change points of bulk force output function

4 | HYBRID NONLINEAR OBSERVER DESIGN

From the theoretical results in Section 3 (Theorem 2), we have seen that since the output function F(SOC) is nonmonotonic, we cannot find a feasible solution to the observer design LMI (16). Attempts in MATLAB to find an LMI solution that works over the entire SOC range of the battery failed, that is, no feasible solutions to (16) existed for the output functions shown in Figure 4. The MATLAB evaluations thus reconfirmed the theoretical result of the output functions being required to be monotonic.

With the monotonicity requirement in mind, the SOC range of the battery can be divided piecewise into different regions in a manner such that in each region the load cell force F(SOC) function is a monotonic function. Such a piecewise division of the SOC range into regions R_1 to R_5 is shown in Figure 4. Note that the boundaries of the regions lie near the slope change points of the force output function. For example, R_4 is a narrow region in which the slope of the output y_2 is close to zero. In this region, only the output y_1 will be used by the observer, since y_2 is nonmonotonic in this region. Regions R_3 and R_5 lie on either side of R_4 and both of these regions can utilize both outputs y_1 and y_2. Both y_1 and y_2 are monotonic in these regions.

It is to be noted that in regions R_2 and R_4 the force measurement is nonmonotonic and the voltage function has low sensitivity. However, these regions are narrow and for the rest of the operation range, the combined system does have adequate sensitivity.

It should be noted that we have the liberty of relying on only one of the output measurements in the narrow regions with zero slope, because even with one output the system is still observable, although the result of estimation will not be as accurate as the case when we use both outputs, due to the low sensitivity of V_{oc}(SOC). Hence, the width of these regions was kept narrow so as to minimize regions in which only one output is used by the observer. While it is ideal to have these regions to be as narrow as possible, in practice their width is determined by the accuracy of the measurement models. For example, if we anticipate a considerable horizontal uncertainty or shift in the output functions, we are forced to sacrifice the estimation accuracy for the sake of stability by widening the low observability regions.

It should be pointed out that if the battery were to operate around the R_2 and R_4 regions for sustained periods of time, the estimation accuracy would deteriorate. The estimation method developed in this article relies on these regions being narrow and prolonged operation not occurring in these regions.

A switched gain observer is developed using the regions defined in Figure 4. As shown in Figure 5, the switched gain observer uses different gains in each of the discrete piecewise regions. Since each region R_1 through R_5 has monotonic output function properties, a constant stabilizing observer gain exists in each of these regions. As the operating region changes, the observer gains switch in value accordingly using a finite state machine of the type shown in Figure 5.

In Figure 5, region i has the observer gain L_i, which has been designed using the LMI of Equation (16) and the corresponding value of the Lyapunov positive definite matrix P_i. Likewise, region j has the observer gain L_j and the positive definite Lyapunov function matrix P_j.

The stability of the hybrid observer of Figure 5 consisting of different constant observer gain regions needs to be considered. It should be noted that inside each region, a single observer gain is used and therefore exponential stability is guaranteed inside this region using the Lyapunov function analysis of Theorem 2. However, different regions i may have different values of the matrix $P_i > 0$ in their individual Lyapunov functions. The stability of the overall switched system

FIGURE 5 Finite state machine for switched-gain observer

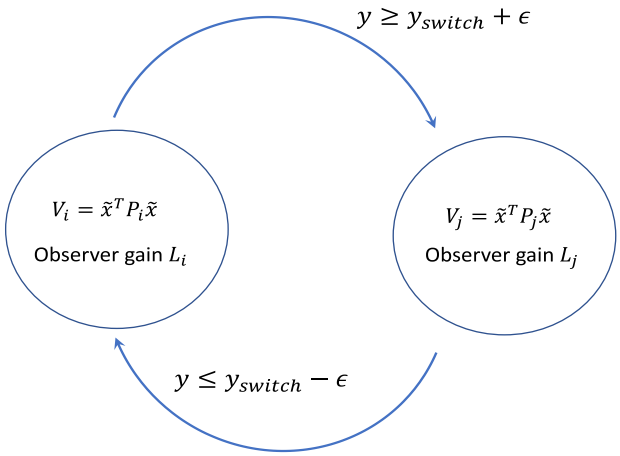

can be guaranteed if the system satisfies a minimum dwell time constraint in each region, according to results from a recent publication.[28] The minimum dwell time in region j when switching from region i to region j needs to be greater than T, where T is the amount of time needed for $V_j(x(t+T)) < V_i(x(t))$. This minimum dwell time guarantees global asymptotic stability.

This result can be understood as follows: In each individual region, the estimation error $\tilde{x}$ keeps decreasing due to the Lyapunov exponentially stable design in that region. In switching between regions, the P matrix may be different in the two regions. However, if the system remains in the same region for a minimum dwell time, the error will become smaller than the initial value at the time the region was entered (due to local exponential stability). Thus, if the system is constrained to remain in one region for a minimum dwell time, the value of the Lyapunov function after the dwell time in region j is less than its value in region i at the time the switch from i to j occurred. This guarantees overall asymptotic stability.[28]

In the case of the observer design application for the SOC estimation system, the values of y at which the region is entered and at which it switches back are different (as shown in Figure 5). This hysteresis between entering and switching back ensures that the minimum dwell time constraint is met.

One obstacle that could affect the performance of this piecewise nonlinear observer is the initial condition. If we pick the initial condition to be in the wrong region (with the wrong observer gain), it might result in a divergence of the observer estimates. However, thanks to the specific shape of output functions for this application, there is an easy solution that can remedy this shortcoming. From Figure 3, since there is a one-to-one relationship between the SOC and the ordered output pair that is constructed by the two output functions y_1 and y_2, we can identify the correct region for the initial condition accurately.

5 | SIMULATION RESULTS

5.1 | Nominal simulations (no model uncertainty in measurement equations)

The estimated SOC from the nonlinear observer is shown in Figure 6 along with the actual SOC for the charge-discharge cycles of Figure 2. As is clear in the figure, the estimated SOC follows the actual values very closely. There are regions in the estimation curve, however, with some apparent deviations from the real value; these are the regions where the observer is only using the terminal voltage in the measurements equation and it is discarding the bulk force measurements that are available (regions R_2 and R_4 around the slope-change points in Figure 4). It is expected that neglecting one of the measurements will reduce the accuracy of the estimation, especially since the only measurement that is being used in these regions contains hysteresis.

Figure 7 shows the error in estimation defined as the difference between the estimated and actual SOC values. The regions where only the terminal voltage is being used is also visible here. The RMS of the error is 0.011 and, ignoring the initial condition part, the maximum error is seen to be 0.036.

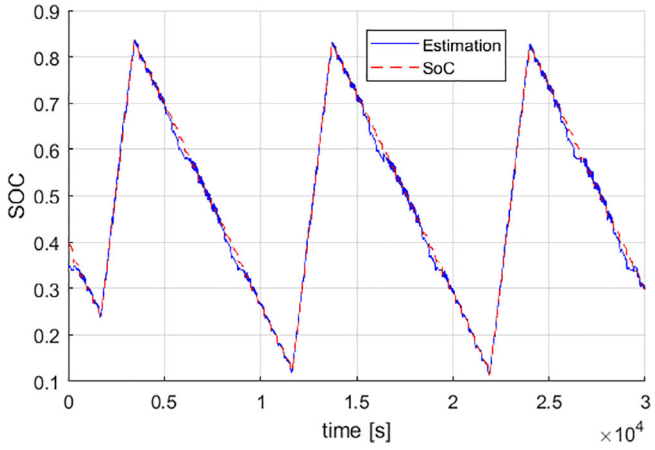

FIGURE 6 Estimated SOC from nonlinear observer along with actual SOC

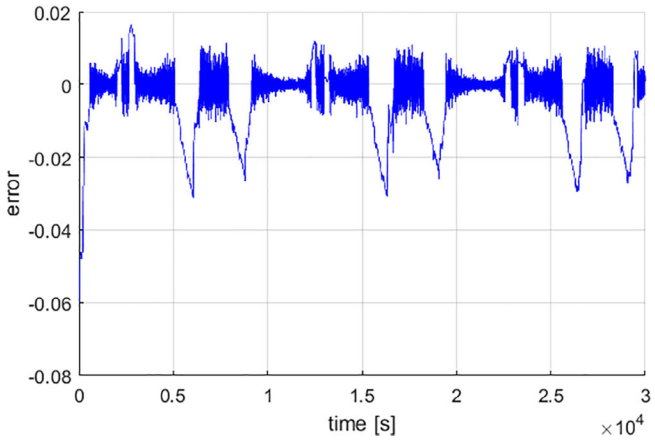

FIGURE 7 Estimation error of the observer

5.2 | Alternative observer with open-loop estimation within the bands

As was stated earlier, the largest amount of error occurs in the bands where the nonlinear observer relies solely on the terminal voltage. One simple solution to this problem is to ignore the measurement altogether in these regions, and instead just use the dynamic equations. This open-loop observer is frequency referred to as the coulomb-counting method in the literature. The results of using such a scheme are illustrated in Figure 8. It can be seen that using the open-loop observer within the slope-change bands improves the estimation in these regions and the RMS of the error has been reduced to 0.007 and the maximum error to 0.02.

It is to be noted, however, that this result is achievable only because of the assumed high accuracy of the dynamic equations (since we are using synthetic measurements with miniscule added noise and bias). Had the bias in current measurement been bigger or were there some larger noise or model uncertainty within the data, this method would have provided deteriorated estimation. In addition, the stability of the observer is no longer guaranteed in this case.

5.3 | Estimation using an extended Kalman filter

The extended Kalman filter can also be used to estimate the SOC of the nonlinear lithium-ion battery system. The result is shown in Figure 9. The estimation is very accurate, which is expected since the synthetic added noise is Gaussian and the extended Kalman filter is close to optimal in this situation. This will not be the case when actual experimental measurements are used and model uncertainty is present. The other issue is that, unlike nonlinear observers, there is no proof of global asymptotic stability in this case. As we will see later, the filter might become unstable with the introduction of model error.

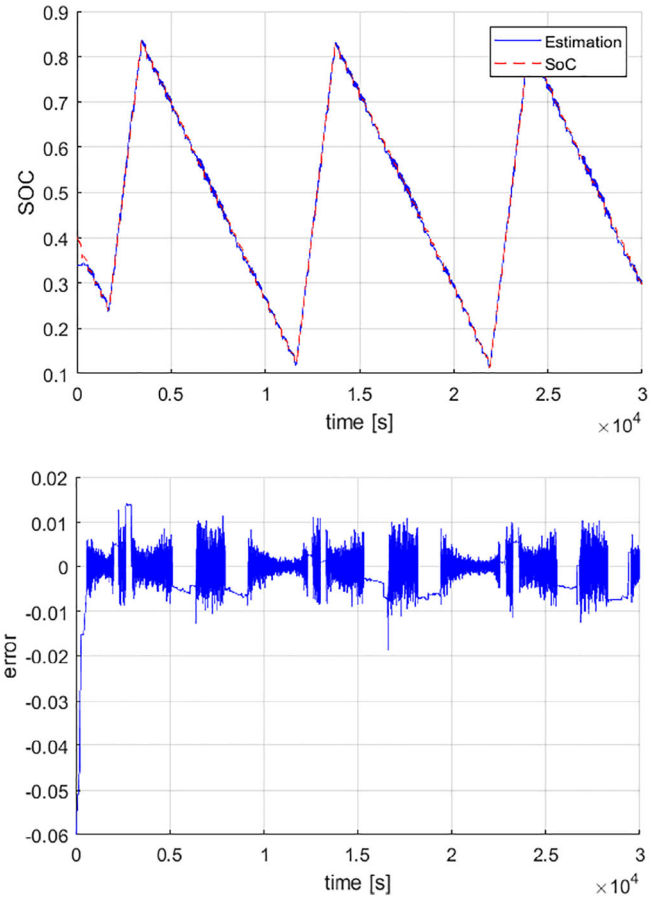

FIGURE 8 Estimated SOC and estimation error of observer where the estimation is done open loop within the slope-change regions

6 | EKF INSTABILITY IN THE PRESENCE OF MODEL ERROR

This section describes the influence of model error on both the EKF and the nonlinear observer. It will be seen that even small model errors cause the EKF to become unstable due to the nonmonotonic nature of the output functions. The nonlinear observer continues to be stable in all cases. The types of model errors used in the simulations here are exactly the variations that would be induced by aging in the battery.[29]

1. *Gain error in force*: Here the force-SOC curve was slightly scaled from the model value using $F = F \times 1.0001$. This is just a 0.1% error in the scaling factor of the output. It is an extremely small error in gain, as seen in Figure 10. However, this small error causes the EKF to diverge significantly from the real SOC values, as seen in Figure 11.

It can be seen that the EKF diverges significantly as the SOC value approaches 0.6 (ie, the slope change point) and then takes a very long time to converge back to the correct estimates. The return to convergence happens after the slope changes again at a SOC of approximately 0.35. The nonlinear observer, on the other hand, never becomes unstable and continues to perform well through the entire range of SOC values, as seen in Figure 12.

2. *Offset error in SOC*: An offset of 0.05 is added to the force-SOC relationship, using $F = f(\text{SOC} + 0.05)$.

The resulting difference between the actual and modeled force-SOC curves is seen in Figure 13.

Again, the EKF diverges for this model error scenario and never converges back. Hence its simulation results are not explicitly shown here. The performance of the nonlinear observer for this same model error scenario is shown in Figure 14A,B. Again, the nonlinear observer remains stable through the entire charging-discharging scenario (Figure 14A), and it RMS error as seen in Figure 14B is only 0.0521, even with this model error.

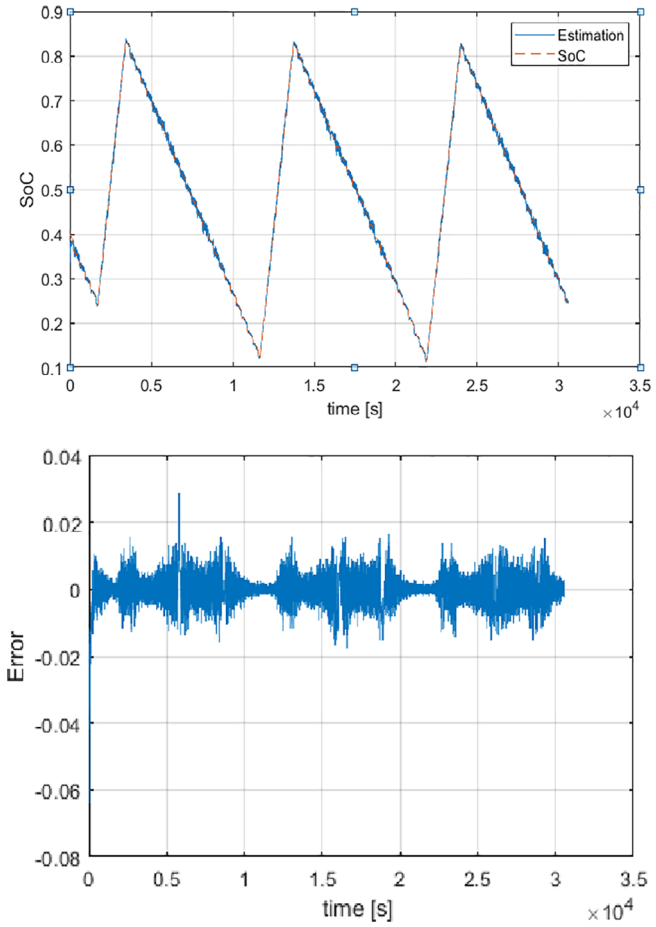

FIGURE 9 Results of EKF estimation

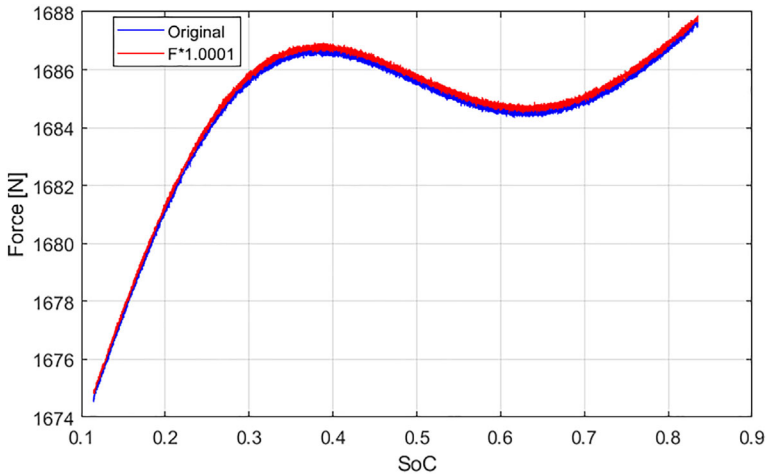

FIGURE 10 Small error in gain for force output curve

3. *Model error at slope-change points*: Minor errors in the slope change points were introduced by slightly modifying the polynomial models for the force-SOC curves. The errors introduced can be seen in Figure 15.

Again, the EKF estimates diverge significantly from the actual SOC values and are therefore not shown. On the other hand, the nonlinear observer continues to remain stable and performs accurately, as seen in Figure 16.

It is to be noted that the EKF could be made more robust by incorporating the same logic as the hybrid observer, that is, to use only voltage in regions R2 and R4 and both outputs in regions R1, R3, and R5. Since the EKF uses varying gain it should have automatically adjusted gains based on the sensitivity of the output nonlinear functions, since it uses the

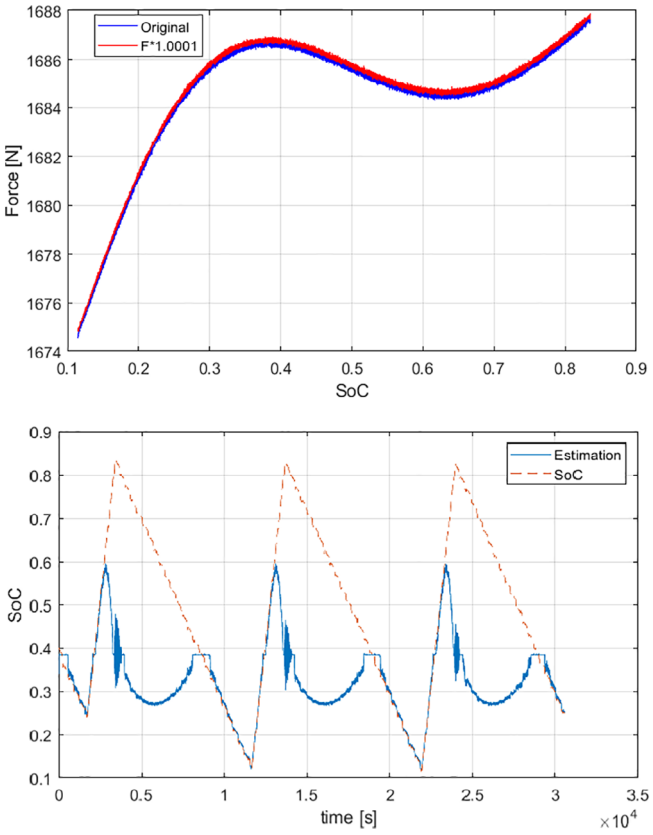

FIGURE 11 Results of EKF estimation with scaling factor error of 0.1%

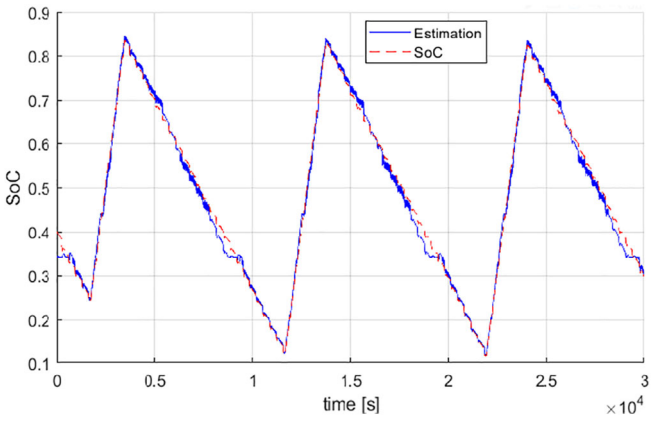

FIGURE 12 Results of nonlinear observer estimation with scaling factor error of 0.1%. The RMS error is 0.015

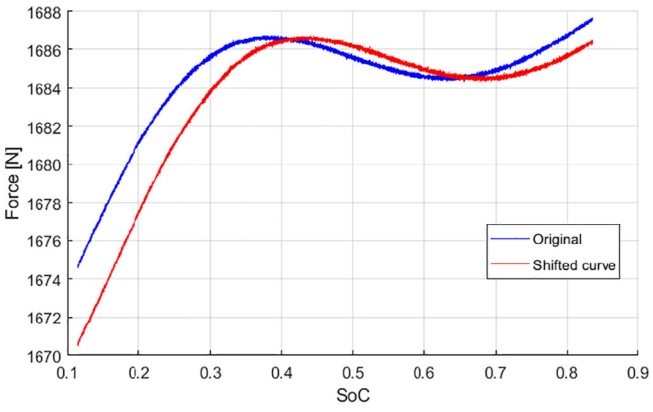

FIGURE 13 Force output curve with a lateral shift in SOC of 0.05

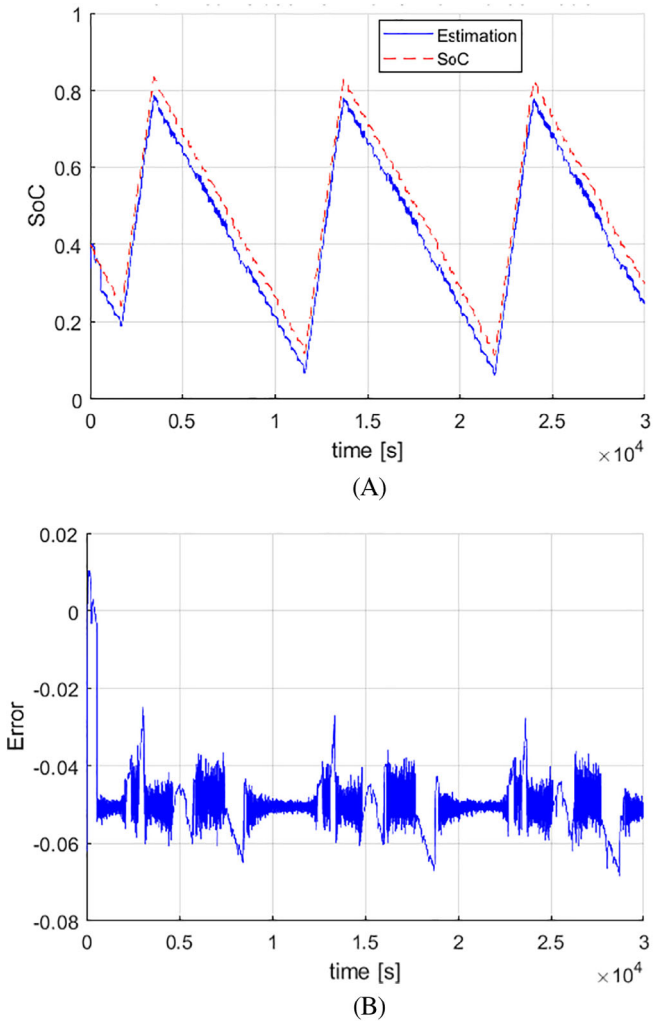

FIGURE 14 Results of nonlinear observer estimation with lateral offset in SOC

Jacobian of the nonlinear function in determining the gain. However, this automatic adjusting of the time-varying gains does not seem to be sufficient to provide robustness.

7 | ROBUSTNESS TO INITIAL CONDITION ERRORS

For the hybrid nonlinear observer to be guaranteed to remain stable, the region of the initial condition needs to be identified correctly, so that the correct initial observer gain is chosen. If the initial region is identified incorrectly, then the use of the wrong observer gain can lead to instability. One way to identify the initial region is based on the simultaneous measured values of the two-ordered outputs, that is, force and terminal voltage. Figure 17 shows how the initial condition can be identified to be in one of five regions, based on the values of force and voltage. For simplicity and a test of robustness, the observer assumes that the initial condition is the midpoint of the region, which has been identified as the initial region. Starting from this initial value, the estimates will converge to the correct values due to the stability of the observer. Two examples with different initial conditions are shown in Figure 18. Note that due to the fast convergence of the observer, the initial condition error can only be seen as a very short spike at time zero in some of the plots. As can be seen, when the initial point is in one of the regions where the observer is using both output functions (Figure 18A), the observer converges to the correct SOC value almost instantaneously. But when the simulation starts from a region where only the voltage is being used (Figure 18C), since the sensitivity of the output function is very limited, the convergence takes longer to happen. Even in this case the estimation error will always stay bounded within the region.

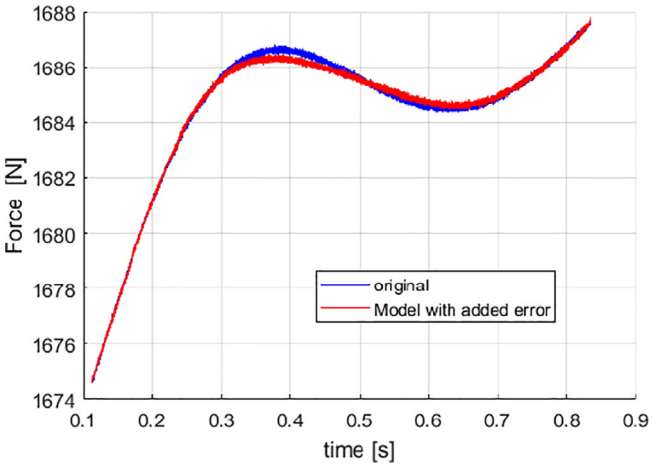

FIGURE 15 Error in slope-change points of force-SOC curve

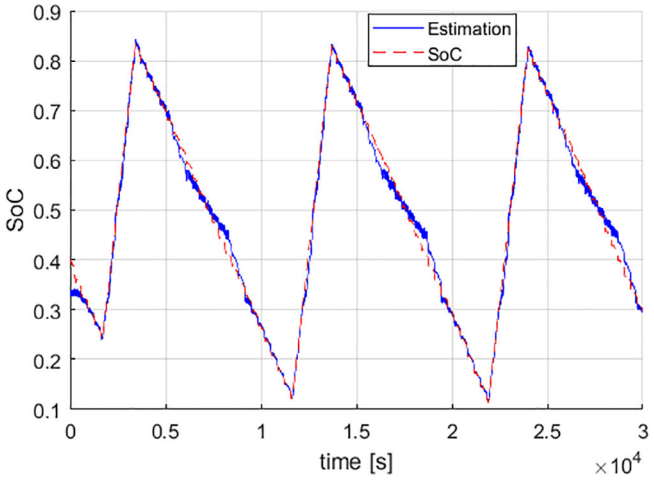

FIGURE 16 Results of nonlinear observer estimation with error in slope-change points

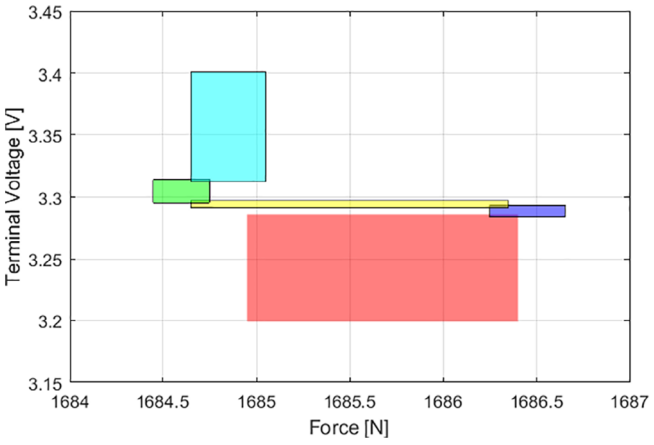

FIGURE 17 The values of force and terminal voltage determine operating region and the related initial condition. Depending on the accuracy of the force and voltage measurements, there could be small areas, which are shared between two regions and could have either of the initial conditions

While the width of the regions (bands) with solely voltage output was widely assumed to be 0.1 of SOC here, in practice it can be minimized based on the accuracy of the bulk force model in experimental data, and hence the convergence can be improved. Furthermore, gridding the domain, instead of picking the middle point of the entire region as the unknown initial condition, could further improve the convergence in the regions with limited sensitivity.

Depending on the accuracy of measurement, we might have intervals in which the initial condition could belong to either of two neighboring regions (Figure 17). By picking the observer gains conservatively, we can ensure that choosing either of the regions would guarantee stability.

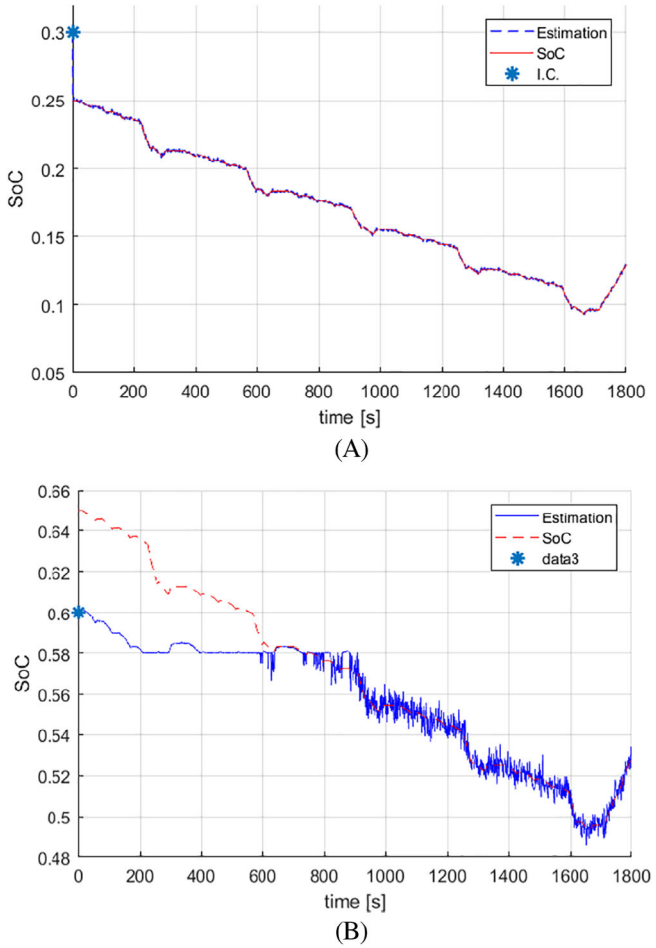

FIGURE 18 SOC estimation and true value for different initial conditions. A, Initial SOC = 0.25, initial observer guess = 0.3. B, Initial SOC = 0.65, initial guess: 0.6

A more robust initial condition determination method can be obtained if the numerical first- and second-order derivatives of the outputs are used, in addition to their raw values. Since change in SOC happens very slowly, numerical values of first and second derivatives can be obtained accurately using a few time samples of data, if the sampling frequency is fast.

8 | EXPERIMENTAL PERFORMANCE

The developed nonlinear observer and the EKF were both evaluated using experimentally measured data from the University of Michigan battery test rig instrumented with sensors that measure terminal voltage, current, and load cell force.[4] A small bias error was added to the current signal to represent an inexpensive current sensor that would normally be available on a commercial battery.

Figure 19 shows the force as a function of SOC for the battery during a number of charge-discharge cycles. The charge-discharge cycles can be seen in Figure 20. While the experimental force-SOC curve in Figure 19 clearly shows a hysteresis type of phenomenon, the curve is modeled using just a single polynomial without hysteresis (shown by the dashed red curve in the figure).

Figure 20 shows the performance of the nonlinear observer in estimating the SOC. It can be seen that the SOC is estimated quite well in spite of the large hysteresis error in the force-SOC model (as well as in the V_{oc}(SOC) model). The error is typically seen to be within 2% for most of the operation, but rises to have a spike of 6% at the points, where a switch from charging to discharging, or vice-versa, occur (due to hysteresis).

The performance of the nonlinear observer can be compared with that of the EKF, which is seen in Figure 21. Due to the hysteresis and the error in the zero-slope points of the model vs the actual data, the EKF often diverges completely from the actual SOC, just as it did in the simulations.

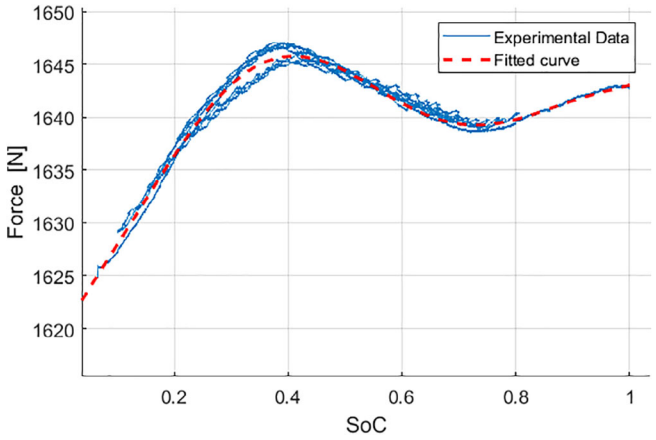

FIGURE 19 Measured experimental force-SOC curves and corresponding single polynomial model

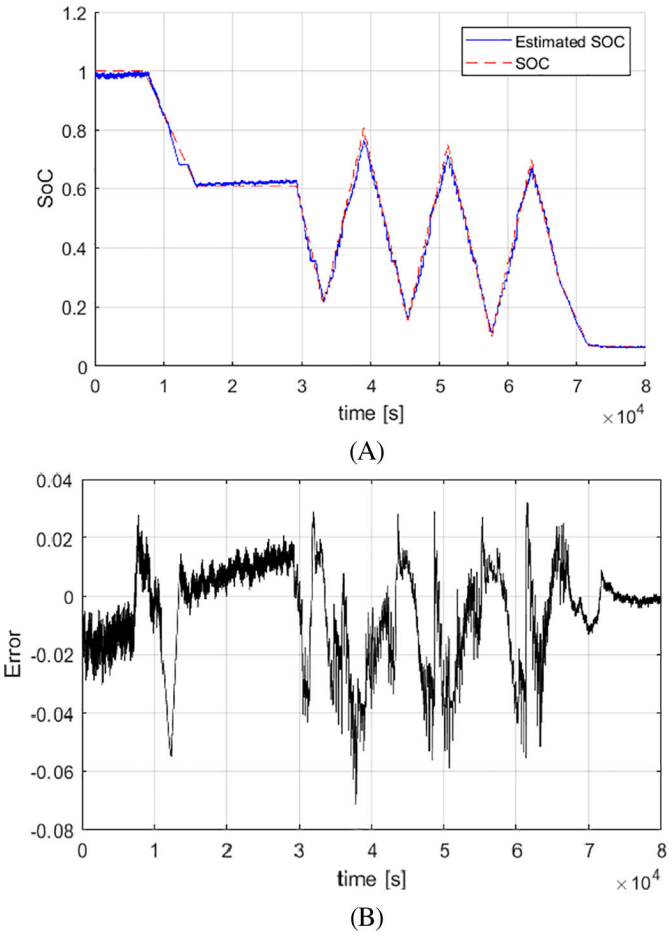

FIGURE 20 Actual and estimated SOC with nonlinear observer during charge-discharge cycles

To prevent the EKF from divergence, the sensor noise covariances during EKF design can be highly amplified so that the EKF feedback gain will be very small and the EKF estimation will largely rely on the model rather than on sensor feedback. This aspect is shown in Figure 22. Here, it can be seen that the EKF estimates no longer diverge from the actual SOC values. However, they do suffer from a drift due to the small bias error in current measurement and no corrections from the output due to high sensor noise covariance. The nonlinear observer is not affected by the current bias error because it continues to use the voltage and force measurements and relies not only on the model but also on the sensor measurements.

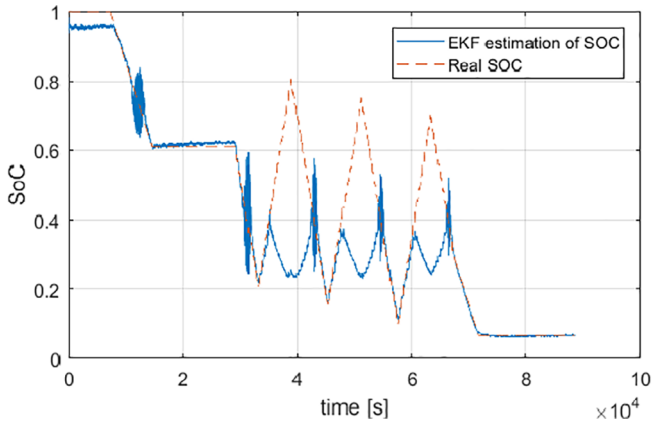

FIGURE 21 Divergence of EKF for the experimental data

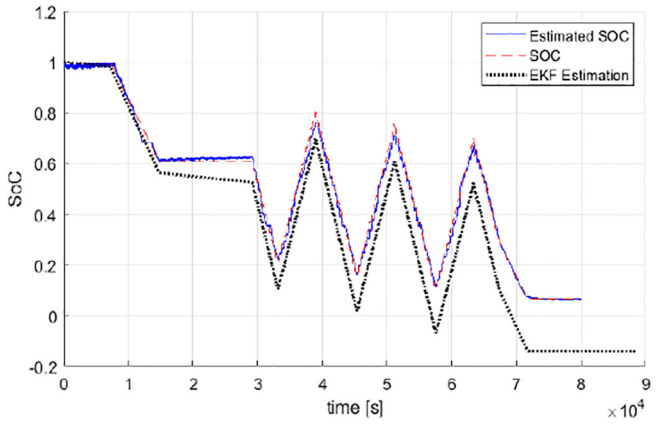

FIGURE 22 Estimates of the nonlinear observer and of the EKF in the presence of measurement bias, when sensor noise covariances are chosen to be extremely large for the EKF

9 | CONCLUSIONS

This article developed a hybrid nonlinear observer for SOC estimation in a lithium-ion battery, using measurements of terminal voltage and bulk force. While both outputs are nonlinear functions of SOC, the force is a highly nonmonotonic function. The nonmonotonicity of the force-SOC curves poses a special challenge for observer design.

The basic nonlinear observer for this system was designed using Lyapunov analysis relying on lower and upper bounds of the Jacobian of the nonlinear output function. Rigorous analysis showed that the proposed nonlinear observer may only have feasible design solutions when the output is monotonic (ie, in each piecewise monotonic region of the output function). It has no constant observer gain feasible solution when the entire SOC range is considered. Furthermore, several other nonlinear observer design methods from literature were also shown to fail in designing a stable observer with a feasible observer gain for this application. The nonmonotonicity challenge was then addressed by designing a hybrid nonlinear observer that switches between several constant observer gains. In each constant-gain region, the observer is designed to be stable using a Lyapunov function and an LMI-based design technique. The overall stability of the switched system is guaranteed by ensuring overlap between regions and an adequate dwell time between switches.

The performance of the observer was evaluated first through simulations using a high-fidelity battery model and then through experiments. The performance of the nonlinear observer was compared with that of an extended Kalman filter, which would traditionally be used for SOC estimation. Simulation results with the high-fidelity model showed that with no model uncertainty and not accounting for hysteresis, the nonlinear observer provides estimates with an RMS error of 1.1% and a maximum error of 3.6%. The EKF performs better when there is no model error, providing an RMS error less than 1% and a maximum error of only 2%. However, it has continuously varying gains, unlike the nonlinear observer that switches between only five constant gains.

The nonlinear observer shines when model error is introduced into the system. In the presence of model error in slope change points, the EKF becomes unstable for even very small errors in the output curves. The nonlinear observer, on the other hand, continues to perform very well, providing accurate estimates and never becoming unstable.

The experimental results verified the observations from simulation, and the EKF was found to become unstable due to model errors even in the experimental data, while the hybrid nonlinear observer continued to work reliably for this SOC estimation problem.

In conclusion, it is worth mentioning that the variability of the bulk force vs SOC relationship with temperature and humidity, and its variation with time over the battery life remain to be studied. This article assumed that the expansion with respect to each half-cell is invariant as the cell ages, but a loss in active material or cycleable lithium could cause the shape to change with respect to SOC as the battery ages according to Reference [27]. These studies will be considered by the authors for future work.

ACKNOWLEDGEMENT

This research was supported in part by a research grant from the National Science Foundation (NSF Grant CMMI 1562006).

ORCID

Miriam A. Figueroa-Santos https://orcid.org/0000-0001-5553-6652
Jason B. Siegel https://orcid.org/0000-0003-2824-013X
Rajesh Rajamani https://orcid.org/0000-0001-9931-7419

REFERENCES

1. Chung D, Elgqvist E, Santhanagopalan S. "Automotive Lithium-Ion Battery Supply Chain and US Competitiveness Considerations" No. NREL/PR-6A50-63354. Clean Energy Manufacturing Analysis Center (CEMAC); 2015.
2. Hannan MA, Lipu MSH, Hussain A, Mohamed A. A review of lithium-ion battery state of charge estimation and management system in electric vehicle applications: challenges and recommendations. Renew Sustain Energy Rev. 2017;78:834-854.
3. Lu L, Han X, Li J, Hua J, Ouyang M. A review on the key issues for lithium-ion battery management in electric vehicles. J Power Sources. 2013;226:272-288.
4. Polóni T, Figueroa-Santos MA, Siegel JB, Stefanopoulouet AG. Integration of non-monotonic cell swelling characteristic for state-of-charge estimation. Paper presented at: Proceedings of the 2018American Control Conference (ACC); 2018:2306-2311; IEEE.
5. Chen Z, Fu Y, Mi CC. State of charge estimation of lithium ion batteries in electric drive vehicles using extended Kalman filtering. IEEE Trans Veh Tech. 2013;62:1020-1030.
6. Xiong R, He H, Sun F, Zhao K. Evaluation on state of charge estimation of batteries with adaptive extended Kalman filter by experiment approach. IEEE Trans Veh Tech. 2013;62:108-117.
7. Wang Y, Fang H, Zhou L, Wada T. Revisiting the state-of-charge estimation for lithium-ion batteries - a methodical investigation of the EKF approach. IEEE Control Syst. 2017;37(4):73-96.
8. Mohan S, Kim Y, Siegel JB, Samad NA, Stefanopoulou AG. A phenomenological model of bulk force in a li-ion battery pack and its application to state of charge estimation. J Electrochem Soc. 2014;161(14):A2222-A2231.
9. Mohan S, Kim Y, Stefanopoulou AG. On improving battery state of charge estimation using bulk force measurements. Paper presented at: Proceedings of the ASME 2015 Dynamic Systems and Control Conference; October 2015.
10. Jones EMC, Silberstein MN, White SR, Sottos NR. In situ measurements of strains in composite battery electrodes during electrochemical cycling. Exp Mech. 2014;54(6):971-985.
11. Cannarella J, Leng CZ, Arnold CB. On the coupling between stress and voltage in lithium-ion pouch cells. Energy Harvest Storage Mater Dev Appl V. 2014;9115:91150K.
12. Oh K-Y, Siegel JB, Secondo L, et al. Rate dependence of swelling in lithium-ion cells. J Power Sources. 2014;267:197-202.
13. Samad NA, Kim Y, Siegel JB, Stefanopoulou AG. Battery capacity fading estimation using a force-based incremental capacity analysis. J Electrochem Soc. 2016;163(8):A1584-A1594.
14. Malik R, Abdellahi A, Ceder G. A critical review of the Li insertion mechanisms in LiFePO4 electrodes. J Electrochem Soc. 2013;160(5):A3179-A3197.
15. Arcak M, Kokotovic P. Nonlinear observers: a circle criterion design and robustness analysis. Automatica. 2001;37:1923-1930.
16. Phanomchoeng G, Rajamani R, Piyabongkarn D. Nonlinear observer for bounded Jacobian systems, with applications to automotive slip angle estimation. IEEE Trans Automat Control. 2011;56(5):1163-1170.
17. Boizot N, Busvelle E, Gauthier J. An adaptive high-gain observer for nonlinear systems. Automatica. 2010;46(9):1483-1488.
18. Wang Y, Madson R, Rajamani R. Magnetic sensor based simultaneous state and parameter estimation using a nonlinear observer. Int J Control. 2019;92(11):2639-2646.
19. Plett GL. Extended Kalman filtering for battery management systems of LiPB-based HEV battery packs: Part 1 background. J Power Sources. 2004;134(2):277-292.
20. Fang H, Wang Y, Sahinoglu Z, Wada T, Hara S. State of charge estimation for lithium-ion batteries: an adaptive approach. Control Eng Pract. 2014;25:45-54.

21. Perez HE, Moura SJ. Sensitivity-based interval PDE observer for battery SOC estimation. Paper presented at: Proceedings of the 2015 American Control Conference (ACC); 2015:323-328; IEEE.
22. Hu X, Li S, Peng H. A comparative study of equivalent circuit models for li-ion batteries. J Power Sources. 2012;198:359-367.
23. Perez HE, Siegel JB, Lin X, Stefanopoulou AG, Ding Y, Castanier MP. Parameterization and validation of an integrated electro-thermal cylindrical lfp battery model. Paper presented at: Proceedings of the ASME Conference; Vol. 3, 2012:41-50.
24. Wang H, Huang Y, Khajepour A. Cyber-physical control for energy management of off-road vehicles with hybrid energy storage systems. IEEE/ASME Trans Mechatron. 2018;23(6):2609-2618.
25. Plett GL. Battery Management Systems. Vol 1. Norwood, MA: Artech House Publishers; 2015.
26. United States Council for Automotive Research LLC Usabc electric vehicle battery test procedures manual, Appendix J - detailed procedure. Report of the United States Council for Automotive Research LLC A/HRC/27/37; 1995.
27. Mohtat P, Lee S, Siegel JB, Stefanopoulou AG. Towards better estimability of electrode-specific state of health: decoding the cell expansion. J Power Sources. 2019;427:101-111.
28. Rajamani R, Jeon W, Movahedi H, Zemouche A. On the need for switched-gain observers for non-monotonic nonlinear systems. Automatica. 2020;114(108814).
29. Lee S, Mohtat P, Siegel JB, Stefanopoulou A. Beyond estimating battery state of health: identifiability of individual electrode capacity and utilization. Paper presented at: Proceedings of the 2018 American Control Conference; 2018; Milwaukee, Wisconsin.

SUPPORTING INFORMATION

Additional supporting information may be found online in the Supporting Information section at the end of this article.

How to cite this article: Movahedi H, Figueroa-Santos MA, Siegel JB, Stefanopoulou AG, Rajamani R. Hybrid nonlinear observer for battery state-of-charge estimation using nonmonotonic force measurements. *Advanced Control for Applications: Engineering and Industrial Systems*. 2020;2:e38. https://doi.org/10.1002/adc2.38